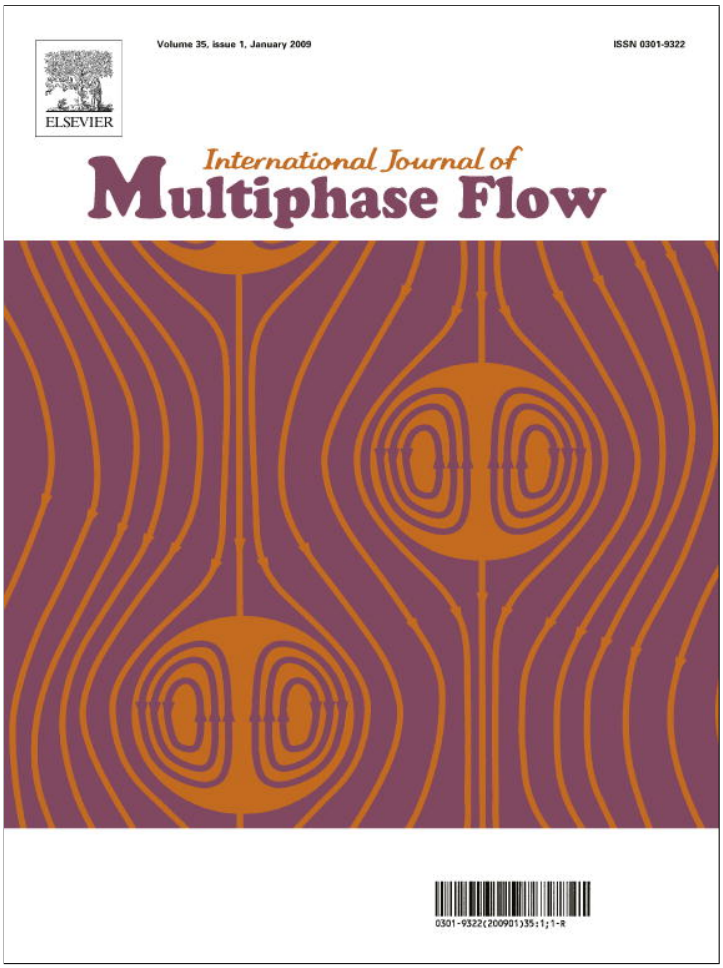

International Journal of Multiphase Flow 35 (2009) 78–90

Contents lists available at ScienceDirect

International Journal of Multiphase Flow

journal homepage: www.elsevier.com/locate/ijmulflow

Nonlinear resonance in viscous films on inclined wavy planes

C. Heining [a,*], V. Bontozoglou [b], N. Aksel [a], A. Wierschem [a,c]

[a] Applied Mechanics and Fluid Dynamics, University of Bayreuth, D-95440 Bayreuth, Germany
[b] Department of Mechanical and Industrial Engineering, University of Thessaly, Pedion Areos, GR-38334 Volos, Greece
[c] Process Systems Engineering, Technische Universität München, Center of Life and Food Sciences Weihenstephan, Weihenstephaner Steig 23, D-85350 Freising, Germany

ARTICLE INFO

Article history:
Received 9 May 2008
Received in revised form 23 July 2008
Accepted 23 July 2008
Available online 12 August 2008

Keywords:
Resonance
Capillary-gravity waves
Free-surface flow
Bottom undulation

ABSTRACT

We study nonlinear resonance in viscous gravity-driven films flowing over undulated substrates. Numerical solution of the full, steady Navier–Stokes equations is used to follow the emergence of the first few free-surface harmonics with increasing wall amplitude, and to study their parametric dependence on film thickness, inertia and capillarity. Bistable resonance is computed for steep enough bottom undulations. As an analytic approach, we apply the integral boundary-layer method and derive an asymptotic equation valid for rather thin films. The analysis recovers the key numerical findings and provides qualitative understanding. It shows that higher harmonics are generated by a nonlinear coupling of the wall with lower-order harmonics of the free surface. It also accounts for bistable resonance, and produces a minimum model whose solution is similar to that of the Duffing oscillator.

1. Introduction

Gravity-driven flow of a thin film down a flat incline is one of the basic flow configurations in hydrodynamics. This system has attracted much attention and has been studied in detail during the last decades. For a review see for instance the monograph by Chang and Demekhin (2002). In most of the industrial and environmental systems, however, the film does not flow over perfectly flat substrates. Thus, it is of great importance to know how the deviations from the perfect condition of a flat incline affect the gravity-driven film flow.

An open issue in the literature is the description of steady flow along a wall with smooth or abrupt topography, i.e. the equivalent of Nusselt solution along a flat incline. The most studied variation of this problem is for negligible inertia and the dominant feature is the formation of separation eddies when the wall undulations are steep enough (Pozrikidis, 1988; Zhao and Cerro, 1992; Wierschem et al., 2003; Wierschem and Aksel, 2004b). Abrupt wall topography (e.g. steps, edges, Aksel, 2000) produces additionally upstream capillary ridges (Kalliadasis et al., 2000; Mazouchi and Homsy, 2001; Davis and Troian, 2005). Other physical effects that have been considered – always in the small Reynolds limit – are the addition of surfactants (Pozrikidis, 2003), thermocapillarity (Kabova et al., 2006), three-dimensionality (Blyth and Pozrikidis, 2006; Luo and Pozrikidis, 2007), wall flexibility (Matar et al., 2007), evaporating films over topography in the lubrication approximation (Gaskell et al., 2006), flow over localized topography (Gaskell et al., 2004) and electrical forces (Tseluiko et al., 2008a, Tseluiko et al., 2008b).

Experiments with increasing inertia (Vlachogiannis and Bontozoglou, 2002; Wierschem and Aksel, 2004a) indicate that the free surface of steady flow becomes progressively more distorted. As the extent of distortion has been found to depend on the height of the corrugations (Argyriadi et al., 2006), a useful theoretical simplification is the linearly undulated wall, with corrugation height much smaller than both corrugation wavelength and thickness of the liquid film. Numerical studies in this linear limit (Bontozoglou and Papapolymerou, 1997; Luo and Pozrikidis, 2006) hint that, for corrugation lengths in the capillary and capillary-gravity regime, the free surface shape is established through a resonant interaction with the wall.

Recently, Wierschem et al. (2008) combined numerical and analytical approaches to carry out a detailed study of linear resonance in arbitrarily thick films. We should note that in their and in the present investigation the notion of resonance is used as a synonym for an amplification of the free surface and film thickness amplitude. The first modes of the Fourier spectrum show linear and nonlinear resonance effects by varying the Reynolds number. Wierschem et al. (2008) showed that resonance is stronger at dimensionless film thickness of about one (scaled with the corrugation wavenumber). For very thin films the free surface approaches the shape of the wall and the resonance maximum flattens around the value one. For very thick films the efficiency of transportation of the bottom perturbation towards the free surface gradually deteriorates. As a result, the resonance remains sharp but declines in amplitude. These authors also concluded that the mechanism of linear

* Corresponding author. Tel.: +49 921 55 7262; fax: +49 921 55 7265.
E-mail address: christianheining@gmail.com (C. Heining).

0301-9322/$ - see front matter © 2008 Elsevier Ltd. All rights reserved.
doi:10.1016/j.ijmultiphaseflow.2008.07.005

resonance involves a phase-locking of the undulated wall with capillary-gravity waves travelling against the mean flow direction.

Despite the convenience of the linear approximation, most applications are expected to involve corrugations of finite height and thus nonlinear effects will gain in significance. Wierschem and Aksel (2004a) observed, in their experiments on film flow over sinusoidal substrates, the generation of higher harmonics and speculated that they might be due to a nonlinear resonance. Vlachogiannis and Bontozoglou (2002) found similar phenomena in film flow over substrates with orthogonal corrugations. Trifonov (1998) and Bontozoglou (2000) studied numerically film flow over sinusoidal corrugations of finite steepness. The latter author observed that with increasing wall amplitude and therefore increasing nonlinearity of the governing equations the resonance curves bend to the right. This bistability with different solution branches and hysteresis is a typical phenomenon in nonlinear resonance.

The experimental and numerical observations mentioned above show distinct features of nonlinear resonance. Yet, there is no understanding of the mechanisms at work in viscous film flow over a wall with corrugations of finite amplitude. In this paper, we combine numerical computations of the steady, full field equations with asymptotic analysis in order to study the qualitative features of the nonlinear resonance. The analysis starts from integral boundary-layer equations and proceeds with a formal small parameter expansion. This approach is complementary to the direct derivation of a nonlinear approximation to the flow based on the dominant eigenvectors (center-manifold theorem), that has provided important results for film flow on a flat wall (Nguyen and Balakotaiah, 2000; Ruyer-Quil and Manneville, 2002) and has recently been extended to a general curved substrate (Roberts and Li, 2006).

Though the present study is limited to steady flow, we note the related stability problem. It is known that, beyond a critical Reynolds number value, film flow becomes convectively unstable to travelling disturbances. The available analytical (Wierschem and Aksel, 2003; Davalos-Orozco, 2007) and numerical (Trifonov, 2007) studies predict that periodic corrugations have a stabilizing effect (i.e. postpone transition to higher Reynolds numbers), and that the stabilizing effect increases with corrugation steepness. These predictions have been experimentally confirmed over a limited parameter range (Wierschem et al., 2005; Argyriadi et al., 2006). We argue, however, that the results of the present steady calculation are important even when corresponding to unstable films. This happens because (i) the steady flow is a prerequisite for stability analysis, (ii) the instability is convective and the steady flow always re-establishes between successive disturbances, and (iii) there is experimental evidence (Argyriadi et al., 2006) that the resonant steady deformation is a dominant characteristic of the unstable free surface and is only slightly modulated in amplitude and phase during the passage of travelling waves.

The outline of the paper is as follows: first, we describe the problem setup in Section 2. In Section 3, we present numerical findings on the generation of higher harmonics and bistable resonance of different harmonics. In Section 4, we derive an analytic equation to study nonlinear resonance. Although the range of validity of this approach is limited to thin films, it allows for a qualitative understanding of the observed nonlinear features, such as the generation of different maxima for higher harmonics as well as a minimal model for the bistability. The results are discussed and summarized in Section 5.

2. Problem setup

We study the steady, two-dimensional film flow of an incompressible and Newtonian liquid down a sinusoidal bottom $y = b(x) \equiv a\cos(2\pi\, x/\lambda)$, with wavelength λ and amplitude a. Axis

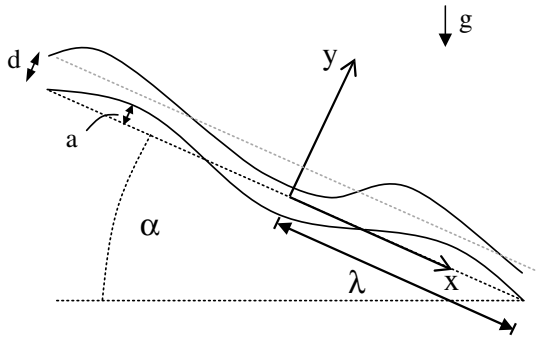

Fig. 1. Film with the Nusselt film thickness d flowing down an undulated bottom profile with wavelength λ, amplitude a and mean inclination angle α. The Cartesian coordinates x and y point in mean flow direction and perpendicular to it.

x is the Cartesian coordinate in main flow direction, which is inclined at an angle α with respect to the horizontal, as shown in Fig. 1. Axis y is the coordinate perpendicular to the flow direction and the location of the free surface is denoted by $y = h(x)$. The liquid has density, kinematic viscosity and surface tension ρ, ν and σ, respectively, and the volumetric flow rate per unit cross-section $\dot{q}$.

The characteristic scales are the film thickness, d, and the mean velocity, $\langle u\rangle$, of steady flow along a flat incline, which are given by the Nusselt solution

$$d = \sqrt[3]{\frac{3\nu\dot{q}}{g\sin\alpha}}; \quad \langle u\rangle = \frac{\dot{q}}{d} = \frac{gd^2\sin\alpha}{3\nu} \tag{1}$$

with g the acceleration of gravity. Using this scaling and denoting dimensionless quantities by capital letters, we arrive at the following form of the continuity and Navier–Stokes equations:

$$\nabla\cdot\mathbf{U} = 0, \tag{2}$$

$$(\mathbf{U}\cdot\nabla)\mathbf{U} = -\nabla P + \frac{1}{Re}\nabla^2\mathbf{U} + \frac{3}{Re}\mathbf{g}. \tag{3}$$

Here, $\mathbf{U} = (U,V)$ is the dimensionless velocity vector, with U and V its components in the x- and y-directions, respectively, P is the dimensionless pressure scaled by $\rho\langle u\rangle^2$ and $\mathbf{g}$ is the dimensionless gravity vector. We have also introduced the Reynolds number, defined as $Re = \dot{q}/\nu = \langle u\rangle d/\nu$. With the scaling above, the dimensionless bottom profile reads $Y = B(X) = \xi\cos(\delta X)$ where we introduced the dimensionless wall amplitude $\xi = a/d$ and the dimensionless film thickness $\delta = 2\pi d/\lambda$. We remark that δ may also be interpreted as the dimensionless wavenumber of the wall undulation. X, Y denote the dimensionless coordinates.

The field equations are complemented with the boundary conditions. These are the no-slip and no-penetration condition at the dimensionless bottom $Y = B(X)$

$$U = V = 0, \tag{4}$$

the kinematic boundary condition at the dimensionless free surface $Y = H(X)$

$$UH_x - V = 0, \tag{5}$$

and the dynamic boundary condition at the free surface

$$\mathbf{n}\cdot\mathbf{T} = \left(\frac{3Bo^{-1}}{\delta^2 Re}\right)K\mathbf{n}. \tag{6}$$

Here, we denote by $\mathbf{n}$ the unit vector normal to the free surface, by K the free surface curvature $K = H_{XX}/(1+H_X^2)^{3/2}$, by $\mathbf{T}$ the stress tensor $\mathbf{T} = -(P - P_{\mathrm{air}})\mathbf{I} + (1/Re)[\nabla\mathbf{U} + (\nabla\mathbf{U})^{\mathrm{T}}]$ with $\mathbf{I}$ the identity matrix

and P_{air} the pressure of the air above. Subscripts denote differentiation with the respective coordinate. We have also introduced the inverse Bond number $Bo^{-1} = (2\pi l_{Ca})^2/(\lambda^2 \sin\alpha)$ with capillary length $l_{Ca} = \sqrt{\sigma/(\rho g)}$. Finally, the inlet and outlet boundary conditions are replaced by the assumption that the flow has the same periodicity as the wall, i.e. it is fully developed.

3. Numerical analysis

The goal of the numerics in the present section is to study fundamental nonlinear interactions between the wall and the free surface and to investigate thoroughly the role of the main flow parameters, i.e. film thickness, Reynolds number and inverse Bond number on the free surface shape. The magnitude of the wavy corrugations is expressed by the dimensionless wall amplitude ξ. Linear resonance, corresponds to a wavy wall with amplitude much smaller than film thickness (Wierschem et al., 2008). In this case, the governing equations can be linearized around the flat bottom solution. We use the shape of the free surface as a diagnostic of the degree of nonlinearity. More specifically, we take the Fourier spectrum of $H(X)$ and examine the magnitude of the first few harmonics. Thus, the emerging nonlinear effects are systematically followed and direct comparison with asymptotic results is made possible.

3.1. Computational procedure

In the present application, we exploit the assumption of periodicity and define the computational domain over only one wall wavelength. The mesh consists of equi-distantly distributed nodes in both the X- and Y-directions. While the X-location of the nodes is known a priori the Y-location evolves during the solution procedure according to the relation $Y = \widehat{Y}[H(X) - B(X)] + B(X)$, where the transformation variable $\widehat{Y}$ is equi-distantly distributed in the interval $[0,1]$.

The imposition of periodic boundary conditions creates an additional degree of freedom, which is removed by fixing either the flow rate or the mean liquid level. We opt for the former, and enforce at the inlet the condition

$$\dot{Q} = \int_B^H U \, dY = 1. \tag{7}$$

We also select arbitrarily the pressure at an inlet location in the liquid, either at the bottom or at the free surface (pressure datum), and treat the air pressure as an additional unknown. This procedure facilitates convergence and is permissible because the air pressure has no dynamical significance and only adds a constant to the actual pressure distribution inside the liquid film. For another example of this fairly standard procedure, see Salamon et al. (1994).

The set of equations and boundary conditions (2)–(7) is solved by a Galerkin finite-element method. The primary unknowns of the flow, which are the velocities U and V, the pressure P and the unknown location of the free surface H, are expanded in each element, respectively, in terms of bi-quadratic, bi-linear and quadratic basis functions. The governing equations, weighted integrally with the basis functions, result in the continuity, momentum, and kinematic residuals, which are evaluated numerically using nine-point Gaussian integration and are solved simultaneously for the unknown nodal values by a Newton–Raphson iterative scheme. A more detailed description of the computational scheme is provided by Malamataris et al. (2002).

3.2. Higher harmonics

We first examine the gradual deviation of the resonance curves from linear behaviour (Wierschem et al., 2008). Fig. 2 shows the amplitudes of the first two free surface harmonics as functions of the Reynolds number, for two different values of the wall amplitude. All other parameters were held constant at the values $\alpha = 13°$, $Bo^{-1} = 12.75$, $\delta = 0.35$. The amplitudes of the free-surface harmonics are normalized with the amplitude of the wavy wall and will be denoted as the relative amplitudes in the following. The linear prediction is plotted in Fig. 2(a) as a continuous line. All curves show a local maximum, which corresponds to amplification and will be further referred hereafter as the resonance effect. We observe that the numerical results for $\xi = 0.357$ deviate somewhat from the linear solution, indicating that nonlinearities are already significant. On the contrary, there is good agreement at $\xi = 0.143$, and this wall amplitude is considered as practically linear. The amplitudes of the second harmonics, shown in Fig. 2(b), are generally small, as expected for small deviations from linearity. They both exhibit a local maximum around the resonance Reynolds number of the fundamental harmonic, but the amplitude of $\xi = 0.357$ remains significant at higher Reynolds numbers.

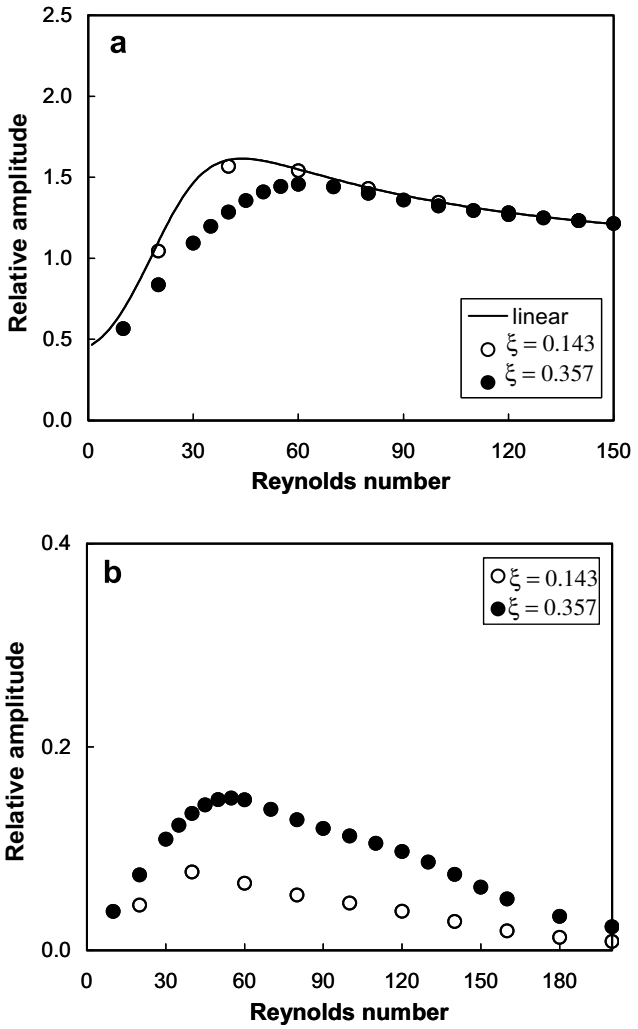

Fig. 2. Numerical calculation of the amplitude of (a) the first and (b) the second harmonic of the free surface, for dimensionless wall amplitude $\xi = 0.143$ (○) and $\xi = 0.357$ (●). The line corresponds to the linear prediction. The other parameter values are: $\alpha = 13°$, $Bo^{-1} = 12.75$, $\delta = 0.35$.

Next, the quantitative characteristics of the second harmonic of the free surface are studied for a vertical wall of small amplitude ($\xi = 0.125$, $\alpha = 90°$), in order to examine the effects of film thickness and inverse Bond number. Initially, the film thickness is held constant at $\delta = 1.0$ and the effect of inverse Bond number is considered.

The amplitude as a function of the Reynolds number is shown in Fig. 3(a) and indicates that at small Bo^{-1} a single peak is observed. With increasing Bo^{-1}, a shoulder appears to the right of the main peak and then separates completely and moves to higher Reynolds numbers. The maximum amplitudes of the two peaks are shown in Fig. 3(b). The primary peak first increases with Bo^{-1} and then saturates to a roughly constant value. The secondary peak grows slowly with Bo^{-1} until the saturation of the primary peak, and therefrom increases faster. However, its amplitude is always smaller than that of the primary peak.

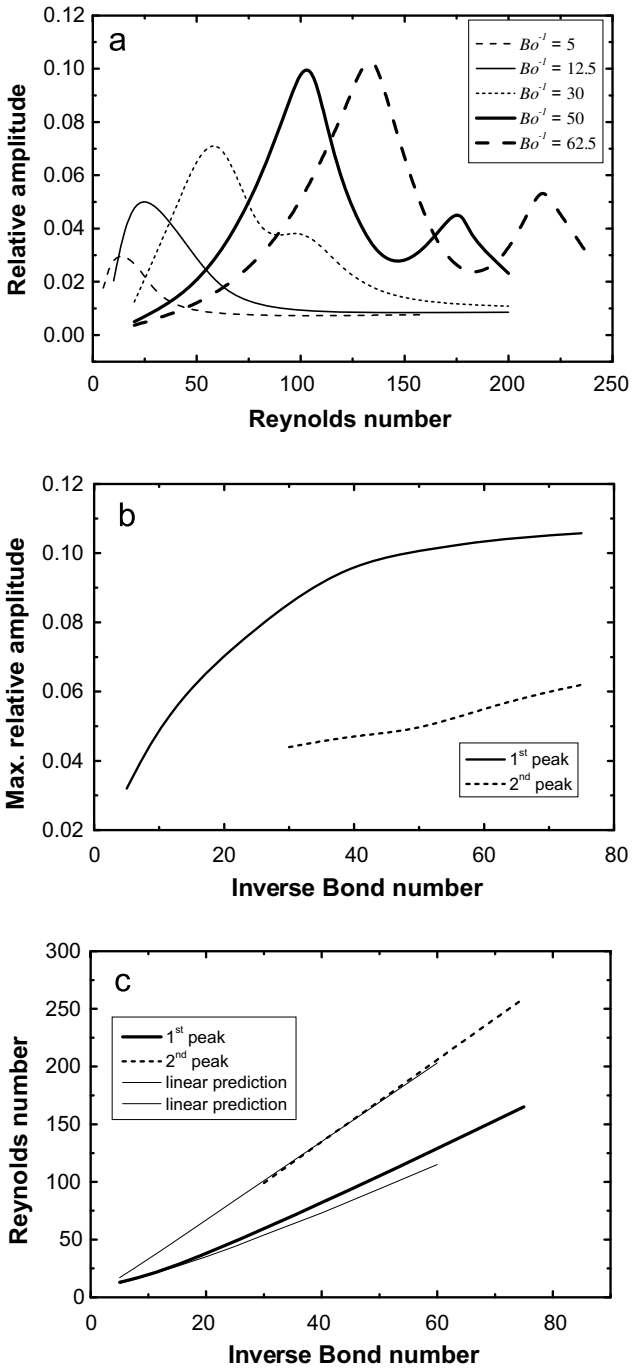

Fig. 3. Amplitude of the second harmonic as a function of the Reynolds number for different inverse Bond numbers (a). Panels (b) and (c) show the amplitudes of the local maxima and the corresponding Reynolds numbers, respectively. The other parameter values are: $\alpha = 90°$, $\delta = 1.0$, $\xi = 0.125$.

Fig. 3(c) shows the Reynolds numbers at which the second harmonic attains the two maxima, and indicates that, with increasing Bo^{-1}, both peaks move to higher Re. These Reynolds numbers are found to coincide with linear predictions of resonance from Wierschem et al. (2008), which are also shown in the figure. More specifically, the lower line (first peak) represents the Reynolds number where linear amplitude becomes maximum, and the upper line (second peak) represents the same prediction but now for a wall with half the wavelength and consequently four times the inverse Bond number ($Bo^{-1} \sim \lambda^{-2}$). These coincidences represent the dominant modes of weakly nonlinear interaction, and will be explained by the asymptotic analysis of the next section.

Next, the inverse Bond number is held constant and the effect of film thickness is considered. Wierschem et al. (2008) have shown that the dimensionless film thickness determines the maximum linear intensity of the resonance: In thin films the linear resonance loses in both sharpness and amplitude, whereas in thick films it diminishes in amplitude while retaining its sharpness. The linear predictions (Wierschem et al., 2008) of maximum amplitude and the Reynolds values where it occurs are reproduced as lines in Fig. 4 for a vertical wall and $Bo^{-1} = 25$ and 100. These are compared with numerical results of the first and second harmonic of the free surface for the weakly nonlinear wall. The maximum in first harmonic is observed to deviate progressively from the linear prediction with decreasing δ, with the deviation aggravating at higher Bo^{-1}. The pertinent Re also deviates with decreasing δ, a behaviour that is reasonable in view of the limitation of linear analysis to $\xi = a/d \ll 1$. The second harmonic has the same qualitative behaviour as the first but is displaced towards lower values of δ. This is also expected, given that the dimensionless film thickness corresponding to the second harmonic is twice the nominal. In all cases, the Reynolds numbers where the first and second harmonics attain maximum values almost coincide.

The behaviour of the third harmonic demonstrates the increase in complexity with the consideration of higher-order effects. We present as an example in Fig. 5 the amplitude of the first three harmonics as function of Re. The third harmonic exhibits three peaks: one at the fundamental resonance, another one at the secondary peak of the second harmonic, and a third one at higher Re. As expected, its magnitude is quantitatively insignificant for such a weakly corrugated wall.

3.3. Bistability

In this section, we study the evolution of the free surface with increasing dimensionless wall amplitude. The main observation relates to the gradual supercritical distortion of the resonance peak, which is a strongly nonlinear effect that becomes quantitatively significant at relatively steep walls. We study again the variation with Re of the first three harmonics of the free surface. As a test case, we consider a vertical wall and the parameter values $Bo^{-1} = 100$ and $\delta = 1.5$, which lead to relatively strong linear resonance.

Fig. 6(a) compares the magnitude of the first harmonic of the free surface for various values of dimensionless wall amplitude. Whereas a weakly nonlinear wall exhibits a vertical peak similar to that predicted by linear analysis, increasing dimensionless wall amplitude leads to the gradual appearance of two solution branches. The left one, starting from low Reynolds numbers extends to a maximum Reynolds number and then ceases to exist. The right one, starting at high Reynolds numbers, exhibits a turning-point bifurcation and meets the left branch at the peak, forming a (very abrupt) second turning point. Thus, with increasing dimensionless wall amplitude, ξ, the resonance peak is strongly skewed to the right.

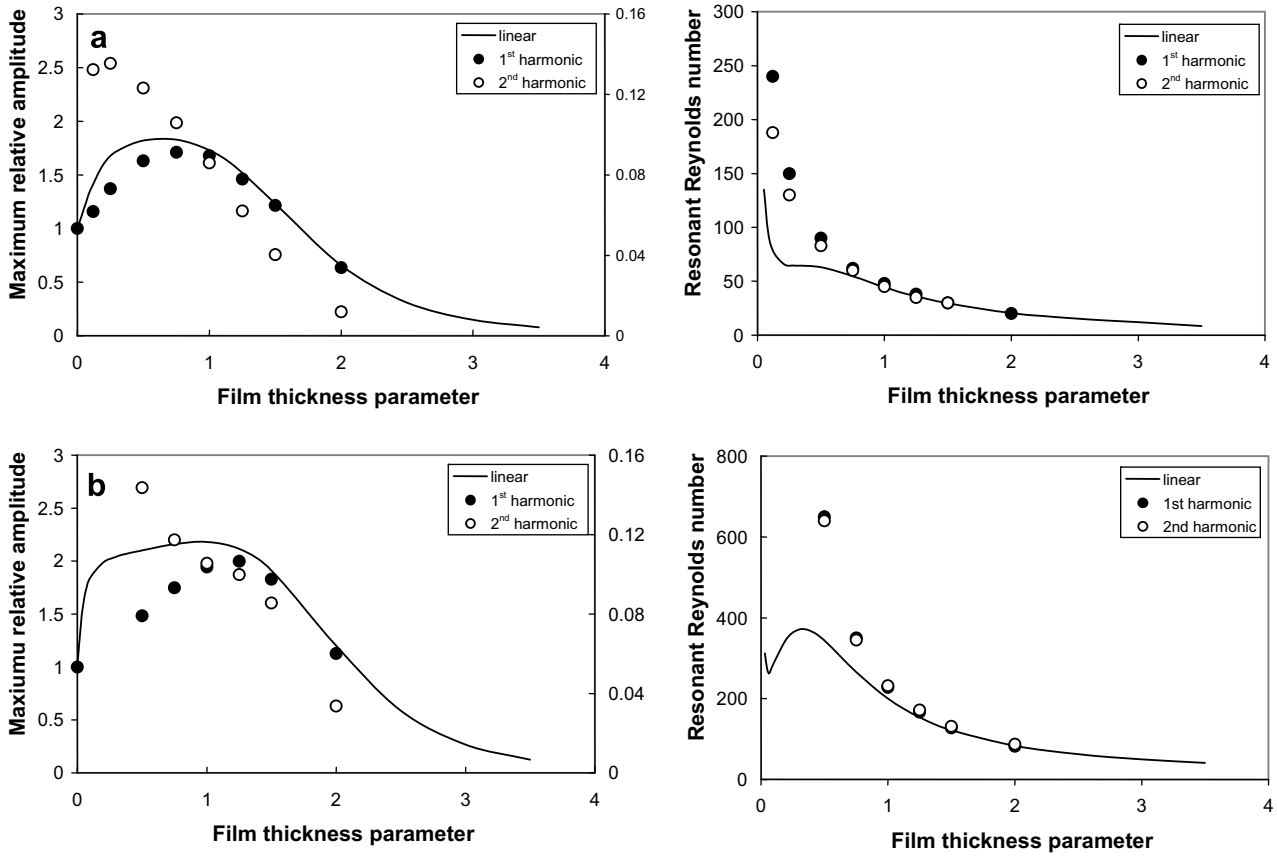

Fig. 4. Numerical calculation of the maximum relative amplitude of the first two free-surface harmonics and of the resonant Reynolds numbers as functions of the film thickness parameter δ for $Bo^{-1} = 25$ (a) and 100 (b) and fixed bottom $2\pi a/\lambda = 0.125$. Lines correspond to the linear prediction. The inclination angle is $\alpha = 90°$. The scale on the right-hand side of the left figures applies for the second harmonic.

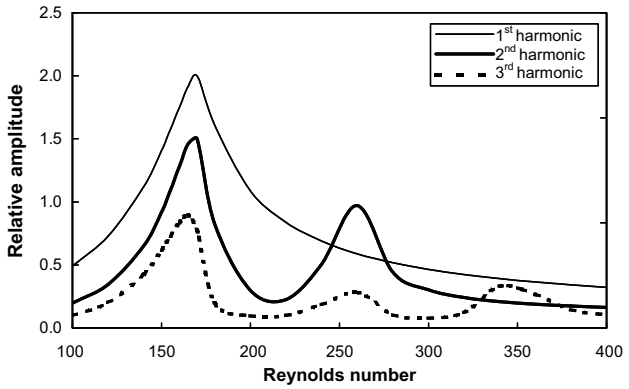

Fig. 5. Amplitude of the first three harmonics as a function of the Reynolds number. The other parameter values are: $\alpha = 90°$, $Bo^{-1} = 100$, $\delta = 1.25$, $\xi = 0.1$.

Fig. 6(b) and (c) show, respectively, the second and third harmonic for the same range of ξ values. It is evident that, with increasing wall amplitude and therefore increasing nonlinearity of the governing equations, bistability gradually becomes significant for higher-order interactions as well. It is also noteworthy that – unlike the first harmonic whose relative amplitude is sharply reduced by the shape distortion of the bistability – the maximum relative amplitudes of the second and third harmonic distinctly increase with dimensionless wall amplitude. For example, quadrupling the dimensionless wall amplitude from $\xi = 0.083$ to $\xi = 0.333$ results at maximum to a doubling of the first harmonic, but to an eightfold increase of the second harmonic. It is concluded that the relative contribution of higher harmonics to the shape of the free surface is magnified with increasing dimensionless wall amplitude.

The above characteristic is brought out in Fig. 7, where free surface profiles are depicted for conditions corresponding to the maximum of second-order resonance and various values of the dimensionless wall amplitude. For $\xi = 0.125$, the free surface is visually indistinguishable from a sinusoidal wave, indicating that the second harmonic is quantitatively insignificant. However, things change drastically with increasing dimensionless wall amplitude and at $\xi = 0.5$ a free surface profile strongly influenced by higher harmonics is predicted. Such free surface manifestation of higher harmonics has indeed been observed in experiments (Wierschem and Aksel, 2004a).

4. Asymptotic analysis

The objective of the present section is to understand the physical mechanisms of the phenomena. We perform an asymptotic analysis and compare the results with the numerics. In thin-film flows the velocity is often well described by a self-similar parabolic velocity profile. Except for steep fronts, this also holds in the presence of surface waves on a flat substrate (Alekseenko et al., 1985; Malamataris et al., 2002) as well as in thin films flowing down wavy planes if the Reynolds number is of order one (Wierschem et al., 2005; Wierschem et al., 2002). Thus we assume a self-similar parabolic velocity profile and use the von Kármán–Pohlhausen integral boundary-layer method to derive an ordinary differential equation for the film thickness. This approach has successfully been applied in various regimes. Shkadov (1967) was the first

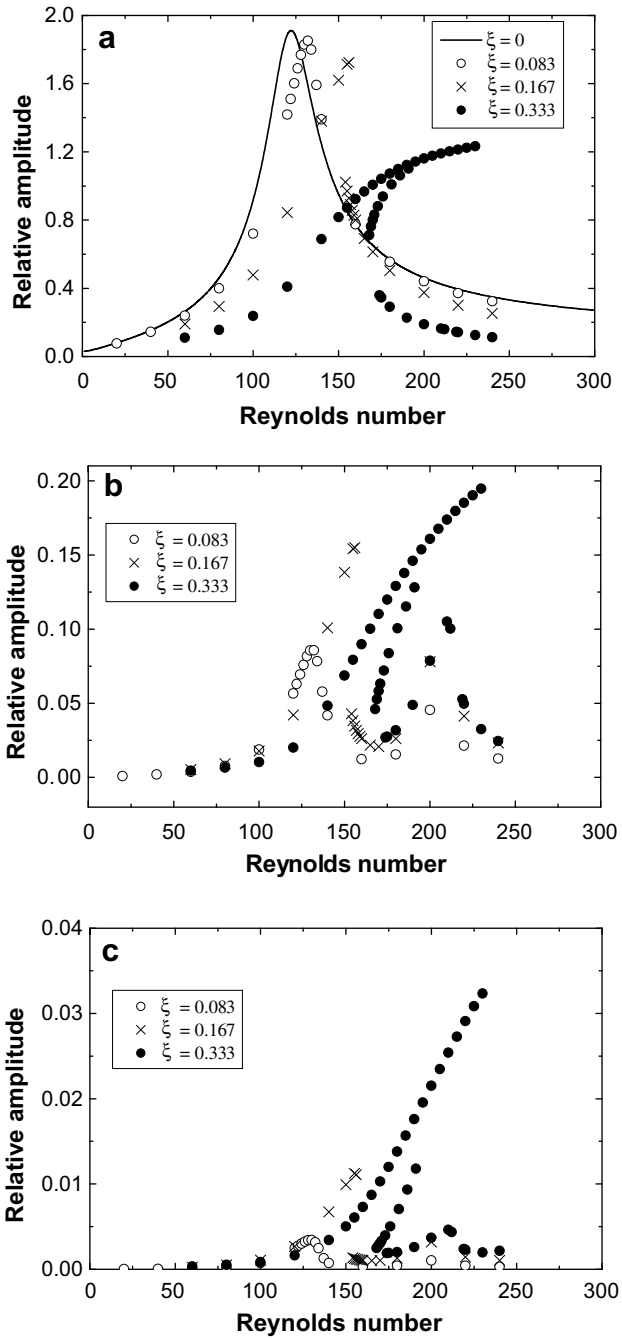

Fig. 6. Panel (a) shows the amplitude of the first harmonic as a function of the Reynolds number for different values of the dimensionless wall amplitude. Panels (b) and (c) show the second and third harmonics, respectively. The other parameter values are: $\alpha = 90°$, $Bo^{-1} = 100$, $\delta = 1.5$.

who derived an integral boundary-layer equation for the flow over a flat substrate. Prokopiou et al. (1991) developed a higher-order theory to investigate surface waves and Uecker (2004) studied nonlinear stability of the integral boundary-layer equations. Trifonov (1998) adapted Shkadov's approach to a periodic bottom profile and Valluri et al. (2005) applied this theory to flow over structured packings.

4.1. Derivation of the resonance equation

We use the following scaling in order to derive the thin-film equation:

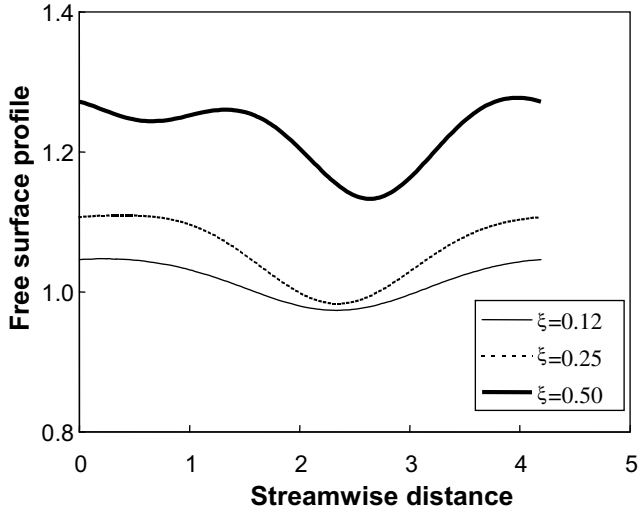

Fig. 7. Free-surface profiles for conditions corresponding to the maximum of second-order resonance and various values of the dimensionless wall amplitude. The other parameter values are: $\alpha = 90°$, $Bo^{-1} = 100$, $\delta = 1.0$.

$$x = \frac{\lambda}{2\pi}X, \quad y = dY, \quad f = dF,$$
$$h = dH, \quad b = aB, \quad p = \rho\langle u\rangle^2 P, \tag{8}$$
$$u = \langle u\rangle U, \quad v = \frac{2\pi d}{\lambda}\langle u\rangle V.$$

With respect to the problem setup in Section 2, we note that an additional variable, the local film thickness $f(x) = h(x) - b(x)$, is introduced and that variables x, b and v are now scaled differently. However, the same dimensionless symbols are retained for simplicity in notation. With the above scaling, the Navier–Stokes equations read in dimensionless form

$$\delta Re\left(U\frac{\partial U}{\partial X} + V\frac{\partial U}{\partial Y}\right) = -\delta Re\frac{\partial P}{\partial X} + 3 + \delta^2\frac{\partial^2 U}{\partial X^2} + \frac{\partial^2 U}{\partial Y^2} \tag{9}$$

and

$$\delta^2 Re\left(U\frac{\partial V}{\partial X} + V\frac{\partial V}{\partial Y}\right) = -Re\frac{\partial P}{\partial Y} - 3\cot\alpha + \delta^3\frac{\partial^2 V}{\partial X^2} + \delta\frac{\partial^2 V^2}{\partial Y}, \tag{10}$$

while the continuity equation takes the form

$$\frac{\partial U}{\partial X} + \frac{\partial V}{\partial Y} = 0. \tag{11}$$

In integral form mass conservation yields the dimensionless flow rate

$$\dot{Q} = \int_{\xi B}^{H} U\,dY. \tag{12}$$

The boundary conditions at the bottom ($Y = \xi B \equiv \xi\cos X$) are the no-slip and no-penetration condition:

$$U = V = 0. \tag{13}$$

At the free surface $Y = \xi B + F \equiv H$ where F is the dimensionless film thickness the kinematic boundary condition reads

$$U\frac{\partial H}{\partial X} - V = 0. \tag{14}$$

Neglecting the viscosity of air, we obtain for the dynamic boundary condition normal to the free surface

$$Re(P-P_{\mathrm{air}})+3Bo^{-1}\frac{\frac{\partial^2 H}{\partial X^2}}{\left[1+\delta^2\left(\frac{\partial H}{\partial X}\right)^2\right]^{3/2}}=2\delta\frac{\partial V}{\partial Y}-\delta\frac{\partial H}{\partial X}\left\{\delta^2\frac{\partial V}{\partial X}+\frac{\partial U}{\partial Y}\right\}. \tag{15}$$

The dynamic boundary condition tangential to the free surface reads

$$\left\{1-\delta^2\left(\frac{\partial H}{\partial X}\right)^2\right\}\left\{\delta^2\frac{\partial V}{\partial X}+\frac{\partial U}{\partial Y}\right\}+4\delta^2\frac{\partial H}{\partial X}\frac{\partial V}{\partial Y}=0. \tag{16}$$

We remark that Re and Bo^{-1} are defined as introduced in Section 2. Since we focus here on thin films, we assume that δ^2 is sufficiently smaller than one to serve as a perturbation parameter. Here, the other geometric parameter, ξ, is treated as a finite fixed value of order one. We expand all quantities in $\delta^2 \ll 1$ and assume that δRe, $\delta\cot\alpha$ and δBo^{-1} are of order one. This allows us to describe fluids with moderate Reynolds and inverse Bond number. Thus, inertia and capillarity occur in the leading order equations. We note that we skip the subscripts of the expansion and from now on all variables denote the leading order in δ^2. With $\delta^2 \ll 1$ (10) reduces to the hydrostatic balance equation and can be integrated using the dynamic boundary condition (15). Eliminating the pressure from (9) we then arrive at

$$\delta Re\left(U\frac{\partial U}{\partial X}+V\frac{\partial U}{\partial Y}\right)=3\delta Bo^{-1}\frac{\partial^3 H}{\partial X^3}-3\delta\cot\alpha\frac{\partial H}{\partial X}+3+\frac{\partial^2 U}{\partial Y^2}. \tag{17}$$

Eq. (17) is complemented by the dynamic boundary condition tangential to the free surface

$$\frac{\partial U}{\partial Y}=0, \tag{18}$$

and the kinematic boundary condition at the free surface

$$U\frac{\partial H}{\partial X}=V, \tag{19}$$

together with the no-slip and no-penetration condition at the bottom:

$$U=V=0,\quad Y=\xi B(X). \tag{20}$$

Using the von Kármán–Pohlhausen integral boundary-layer method (von Kármán, 1921; Pohlhausen, 1921; Spurk and Aksel, 2007), we obtain a single equation for the resonance capillary-gravity waves with the bottom corrugation. Integrating the continuity equation (11) over the film thickness and taking into account (12)–(14) yields

$$\frac{\partial\dot{Q}}{\partial X}=0. \tag{21}$$

Integrating now the momentum equation in X-direction (17) from the bottom to the free surface results in

$$\delta Re\left(\frac{\partial}{\partial X}\int_{\xi B}^{H}U^2\,\mathrm{d}Y\right)=3\delta Bo^{-1}\frac{\partial^3 H}{\partial X^3}F-3\delta\cot\alpha\frac{\partial H}{\partial X}F+3F-\left.\frac{\partial U}{\partial Y}\right|_{Y=\xi B}, \tag{22}$$

where we used integration by parts in the Reynolds term, the no-slip condition at the bottom (13), and the kinematic boundary condition at the free surface (14), and further eliminated $\partial V/\partial Y$ by applying the continuity equation (11). Together with (21), this equation forms a set of two equations.

A specific profile must now be imposed in the theory. According to the discussion in the beginning of the present section, we assume here a self-similar parabolic velocity profile (von Kármán, 1921; Pohlhausen, 1921). Taking into account (12) and (21) the velocity component in X-direction reads

$$U=\frac{3}{F}\left(\frac{Y-\xi B}{F}-\frac{(Y-\xi B)^2}{2F^2}\right). \tag{23}$$

From (22) we obtain with the velocity profile (23) at leading order in δ^2

$$0=\frac{6}{5}\delta ReF_X-3F^3(\delta\cot\alpha F_X-\delta Bo^{-1}F_{XXX})+3(F^3-1)+3(\delta\cot\alpha+\delta Bo^{-1})\xi F^3\sin X. \tag{24}$$

The physical origins of the terms of this nonlinear ordinary differential equation for the film thickness are, in that order, inertia, hydrostatic and capillary pressure, gravity-driven forcing, wall-shear stress. The periodic inhomogeneity is due to the change of the hydrostatic and capillary pressures, respectively, that are caused by the undulated bottom.

In what follows, we expand the film thickness F in a power series of the parameter $\xi \ll 1$:

$$F=F_0+\xi F_1(X)+\xi^2F_2(X)+\xi^3F_3(X)+\mathrm{O}(\xi^4). \tag{25}$$

We note that expanding first the field equations in $\delta^2 \ll 1$ and afterwards expanding the film thickness in $\xi \ll 1$ is a double expansion where the internal orders of magnitudes between the perturbation parameters have to be considered. Keeping n terms in the expansion (25) asymptotic consistency and the physical meaning of the solution is maintained provided that $\xi^{n-1} \gg \delta^2$. In the figures presented in this and in the following sections, we will not always strictly hold this restriction. Asymptotic theories often deliver good results for parameters exceeding the validity domain. A justification will be given by a comparison to the numerical solution.

With this expansion, the nonlinear equation (24) degenerates into a hierarchy of linear ordinary differential equations. The expansion yields for the leading order term $F_0 = 1$, i.e. the steady film thickness for a flat incline.

At first order we obtain from (24)

$$0=\delta\cot\alpha F_{1X}-\delta Bo^{-1}F_{1XXX}-\frac{2}{5}\delta ReF_{1X}-3F_1-(\cot\alpha+Bo^{-1})\sin X. \tag{26}$$

The film flow has no intrinsic oscillation frequency and the homogeneous solution is an exponential function in space. Demanding that the homogeneous solution remains finite for large distances and periodic for a periodic bottom profile yields a zero homogeneous solution. According to the inhomogeneities, we solve (26) with the following ansatz:

$$F_1=C_1\cos X+S_1\sin X, \tag{27}$$

yielding the constants

$$S_1=\frac{-3(\cot\alpha+Bo^{-1})}{\left(\delta\cot\alpha+\delta Bo^{-1}-\frac{2}{5}\delta Re\right)^2+9},\qquad C_1=-\frac{\left(\delta\cot\alpha+\delta Bo^{-1}-\frac{2}{5}\delta Re\right)(\cot\alpha+Bo^{-1})}{\left(\delta\cot\alpha+\delta Bo^{-1}-\frac{2}{5}\delta Re\right)^2+9}. \tag{28}$$

We note that (28) has the same form as the fix point for the weighted-residual model in Oron and Heining (2008). At second-order (24) yields together with (25)

$$0=\delta\cot\alpha F_{2X}-\delta Bo^{-1}F_{2XXX}-\frac{2}{5}F_{2X}\delta Re-3F_2-3F_1^2-3F_1(\delta Bo^{-1}F_{1XXX}-\delta\cot\alpha F_{1X})-3(\delta Bo^{-1}+\delta\cot\alpha)F_1\sin X. \tag{29}$$

While the homogeneous part in the upper line of Eq. (29) remains identical to that for the linear resonance, the inhomogeneous part

is due to nonlinearities in the film thickness (second line) and due to a coupling between bottom contour and film thickness (third line). Inserting the ansatz for the first-order solution yields together with (26)

$$0 = \delta\cot\alpha F_{2X} - \delta Bo^{-1}F_{2XXX} - \frac{2}{5}F_{2X}\delta Re - 3F_2 + 3M_2 + M\sin 2X + N\cos 2X, \tag{30}$$

with

$$M_2 = S_1^2 + C_1^2,$$
$$M = \frac{3}{5}(S_1^2 - C_1^2)\delta Re + 6S_1C_1, \tag{31}$$
$$N = \frac{6}{5}S_1C_1\delta Re + 3C_1^2 - 3S_1^2.$$

Thus at second order, the inhomogeneities, which come from the coupling of the free surface with the bottom contour and from nonlinearities of the free surface profile, yield a modification of the mean film thickness, i.e. the leading order solution, and second harmonics of the bottom contour. According to the inhomogeneities in (30) we choose the following ansatz:

$$F_2 = M_2 + C_2\cos 2X + S_2\sin 2X, \tag{32}$$

where C_2 and S_2 are constants to be determined. Inserting of (32) into (30) yields

$$S_2 = \frac{KM - LN}{L^2 + K^2}, \quad C_2 = \frac{KN + LM}{L^2 + K^2}, \tag{33}$$

with

$$K = \frac{3}{2}, \; L = \delta\cot\alpha + 4\delta Bo^{-1} - \frac{2}{5}\delta Re. \tag{34}$$

At third order, the inhomogeneities result in a modification of the fundamental mode and in a third harmonic of the bottom contour. Accordingly the inhomogeneities are solved using the following ansatz:

$$F_3 = C_{31}\cos X + S_{31}\sin X + C_{33}\cos 3X + S_{33}\sin 3X. \tag{35}$$

The constants C_{31}, S_{31}, C_{33}, and S_{33} take a similar form as for the first and second-order solutions, i.e.

$$C_{31} = \frac{KN_{31} + L_{31}M_{31}}{K^2 + L_{31}^2}, \quad S_{31} = \frac{KM_{31} - L_{31}N_{31}}{K^2 + L_{31}^2},$$
$$C_{33} = \frac{KN_{33} + L_{33}M_{33}}{K^2 + L_{33}^2}, \quad S_{33} = \frac{KM_{33} - L_{33}N_{33}}{K^2 + L_{33}^2}, \tag{36}$$

with

$$K = \frac{3}{2}, \quad L_{31} = \frac{1}{2}\left(\delta\cot\alpha + \delta Bo^{-1} - \frac{2}{5}\delta Re\right),$$
$$L_{33} = \frac{3}{2}\left(\delta\cot\alpha + 9\delta Bo^{-1} - \frac{2}{5}\delta Re\right). \tag{37}$$

The rest of the contributions are given in Appendix A.

4.2. Linear resonance

Wierschem et al. (2008) studied linear resonance for rather thick films. We consider now linear resonance effects in the integral boundary-layer framework. In the previous section, we expanded the film thickness in powers of the parameter ξ, and obtained the solution for a steady film up to third order in ξ. Eq. (26) shows that, to this order, the inhomogeneities are of the fundamental wave number of the bottom undulation. Due to the inhomogeneous terms, the film thickness varies with the wavelength of the bottom contour. The solution is a linear combination of $\sin X$ and $\cos X$ with coefficients S_1 and C_1 given by (28). S_1 is negative in the entire range of Reynolds numbers and tends to zero at large Reynolds numbers. C_1 is negative for rather small Reynolds numbers. It changes sign at $Re = 2.5(\cot\alpha + Bo^{-1})$ and tends to zero for large Reynolds numbers. The relative amplitude of the film thickness reads $\sqrt{S_1^2 + C_1^2}$ and resonance takes place where the denominator in (28) is minimal at

$$Re_1 = \frac{5}{2}(\cot\alpha + Bo^{-1}). \tag{38}$$

At Re_1 the amplitude of the film thickness is maximized whereas the resonant Reynolds number for the maximum free-surface amplitude is different because one has to take into account the elevation and the phase shift due to the periodic wall. Inserting the definitions of the Reynolds number, the inverse Bond number and the film-thickness parameter δ, and using the Nusselt solution for the mean flow velocity (1) and (38) yields

$$\langle u\rangle^2 = \frac{5}{6}\left(u_G^2 + u_{Ca}^2\right)\frac{2\pi h}{\lambda}, \tag{39}$$

where $u_G = \sqrt{g(\lambda/2\pi)\cos\alpha}$ is the phase velocity of gravity waves and $u_{Ca} = \sqrt{(2\pi/\lambda)(\sigma/\rho)}$ is the phase velocity of capillary waves with the wavelength of the bottom contour in infinitely thick liquid layers. We remark that expanding $\tanh(2\pi h/\lambda)$ in a Taylor series results in $\tanh(2\pi h/\lambda) = 2\pi h/\lambda + O((2\pi h/\lambda)^3)$ and thus we recover the resonance with capillary-gravity waves in liquids of finite thickness at first order in the film-thickness parameter.

At $Re = Re_1$, we have

$$C_1 = 0, \quad S_1 = -\frac{1}{3}(\cot\alpha + Bo^{-1}), \tag{40}$$

and thus

$$F_1 = -\frac{1}{3}(\cot\alpha + Bo^{-1})\sin X. \tag{41}$$

Eq. (41) shows that at resonance the changes in the gravity forcing and in capillary pressure yield a phase shift of $\pi/2$ with respect to the bottom $B = \cos X$. It is noted that the effect of hydrostatic and capillary pressures is expressed by a unique combination, the pressure number $P_{hc} = \cot\alpha + Bo^{-1}$. With δP_{hc} of order one, as in the case of Fig. 8(a), the resonance is mainly governed by S_1. Thus the amplitude increases with the pressure number. The figure also shows the phase shift of the film-thickness with respect to the bottom contour, given by $\arctan(-S_1/C_1)$, where the dotted curve corresponds to the maximum film thickness.

The studies of the preceding sections as well as those cited in the literature have focused on the amplitude of the free surface and not on the film thickness (Bontozoglou and Papapolymerou, 1997; Bontozoglou, 2000; Vlachogiannis and Bontozoglou, 2002; Wierschem and Aksel, 2004a). With the dimensionless bottom contour $B = \cos X$, the position of the free surface up to first order in the Cartesian coordinates is at

$$Y = \xi B + F_0 + \xi F_1 = 1 + \xi a_1\cos(X + \Delta\varphi_1), \tag{42}$$

where we introduced the free-surface amplitude

$$a_1 = \sqrt{(1 + C_1)^2 + S_1^2} \tag{43}$$

and the phase shift between the free surface and the bottom contour

$$\Delta\varphi_1 = \arctan\frac{-S_1}{\sqrt{S_1^2 + (1 + C_1)^2}}. \tag{44}$$

It shows that negative C_1 yields a flattening of the free surface while S_1 always produces an amplitude increase. The maximum free-sur-

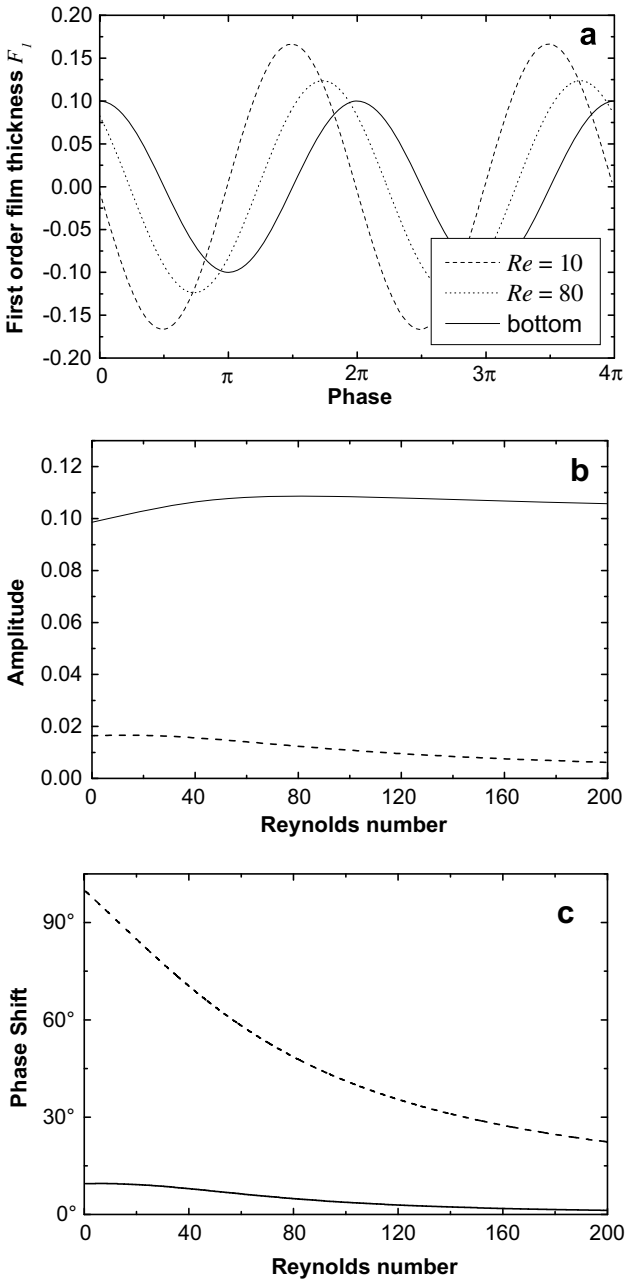

Fig. 8. Panel (a) shows the phase-resolved film thickness F_1 for two different Reynolds numbers. The bottom contour for $\xi = 0.1$ is plotted for comparison. Panels (b) and (c) compare the amplitudes and phase shifts of the film thickness and of the free-surface contour as a function of the Reynolds number, respectively. Dashed and solid curves in (b) and (c) correspond to the maximum film-thickness and free-surface amplitudes, respectively. The other parameter values are: $P_{hc} = 5$, $\delta = 0.1$.

face amplitude also increases with the pressure number and is found to be at

$$Re = \frac{5}{2}\left(P_{hc} - \frac{P_{hc}}{2\delta}\right) + \frac{5}{4\delta}\sqrt{P_{hc}^2 + 36}. \tag{45}$$

For the parameter range considered here, i.e. δP_{hc} being of order one and small δ^2, it is larger than that for the film thickness given by (38).

Fig. 8(b) compares the amplitude of the free surface a_1 to that of the film thickness variation F_1 as a function of the Reynolds number. It shows that the maximum free-surface amplitude is obtained at higher Reynolds numbers than for the maximum film thickness. This is because the decreasing film-thickness amplitude is overcompensated by a decrease in the phase shift between the film thickness and the bottom contour. As shown in Fig. 8(a) and (c), the phase shift between the film thickness at maximum free-surface amplitude and the bottom contour has diminished to about $\pi/4$.

4.3. Nonlinear resonance

The nonlinearity in (24) results in higher harmonic inhomogeneities at higher order in the parameter ξ. In the power expansion, these nonlinearities enter by the coupling of lower-order solutions for the film thickness with each other and with the bottom contour. The second-order solution yields a modification of the mean film thickness and second harmonics of the bottom contour. The mean elevation at second-order M_2 reaches rather large values at low Reynolds numbers and tends to zero at high Reynolds numbers. Eq. (33) shows that the harmonic contribution has the same form as the first-order solution, with L being the resonant term. From (34) results that the amplitude $\sqrt{S_2^2 + C_2^2}$ of F_2 is maximized where L is zero and thus resonance for F_2 takes place at

$$Re_2 = \frac{5}{2}(\cot\alpha + 4Bo^{-1}). \tag{46}$$

Thus, in general the resonance at second order takes place at higher Reynolds numbers than the first-order resonance and coincides with it if surface tension is negligible. Inserting the definitions of the parameters as before for the linear resonance, shows that this corresponds to a resonance with capillary-gravity waves of half the wavelength of the bottom contour:

$$\langle u\rangle^2 = \frac{5}{6}\left(\frac{\lambda/2}{2\pi}g\cos\alpha + \frac{2\pi}{\lambda/2}\frac{\sigma}{\rho}\right)\frac{2\pi h}{\lambda/2}. \tag{47}$$

The resonance, however, takes place only for sufficiently strong M and N terms in (33), i.e. sufficiently strong linear resonance and the nonlinear coupling. Besides this resonance with capillary-gravity waves at half the wavelength of the bottom contour, the second harmonic has a local maximum in the vicinity of the Reynolds number for linear film-thickness resonance. This is due to the strong nonlinear coupling at linear resonance as is apparent from (31). The amplitude of the second-order film thickness and its phase shift are $a_2 = \xi\sqrt{S_2^2 + C_2^2}$ and $\Delta\varphi_2 = \arctan(-S_2/C_2)$, respectively.

Fig. 9(a) shows the influence of the second-order solution on the surface profiles at different Reynolds numbers. For the same parameters, the relative amplitudes of the surface contour at first and second order as a function of the Reynolds number are depicted in Fig. 9(b). It shows that the second-order solution has two local maxima as found in the numerical calculations. The one at higher Reynolds number is due to the higher harmonic resonance (46) and the maximum at lower Reynolds number is due to the coupling to the first-order film-thickness, as the periodic inhomogeneities in (30), M and N, are functions of the first-order solutions S_1 and C_1.

Eq. (46) shows that the resonance at second order moves to higher Reynolds numbers if the inverse Bond number increases. A study of the effect of surface tension on the resonance at second order is shown in Fig. 10. It depicts the free-surface amplitude as a function of the Reynolds number for different inverse Bond numbers. With surface tension being small the second-order solution has a single peak where both effects, the resonance given by (46) and the strong coupling to the first-order solution overlap. The peak augments with increasing inverse Bond number and moves to higher Reynolds numbers. Increasing the inverse Bond number further, the peak splits into two and both of them increase in size and occur at still higher Reynolds number. Thus we recover the same process as observed numerically, see Fig. 3(a).

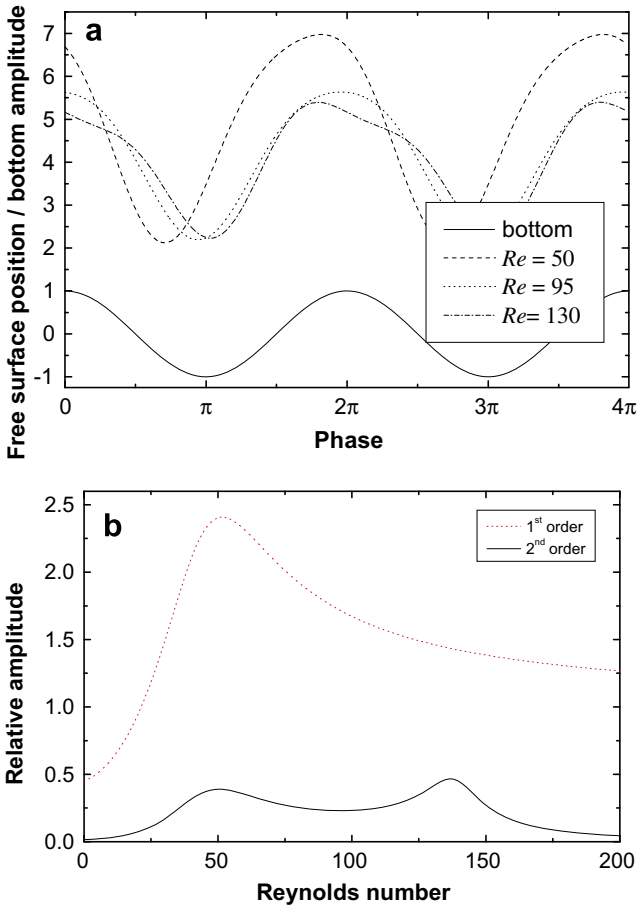

Fig. 9. Free-surface contour including the second-order solution at different Reynolds numbers (a) and second and first-order solutions of the relative free-surface amplitude as a function of the Reynolds number (b). The other parameter values are: $\alpha = 13°$, $Bo^{-1} = 12.75$, $\delta = 0.35$, $\xi = 0.25$.

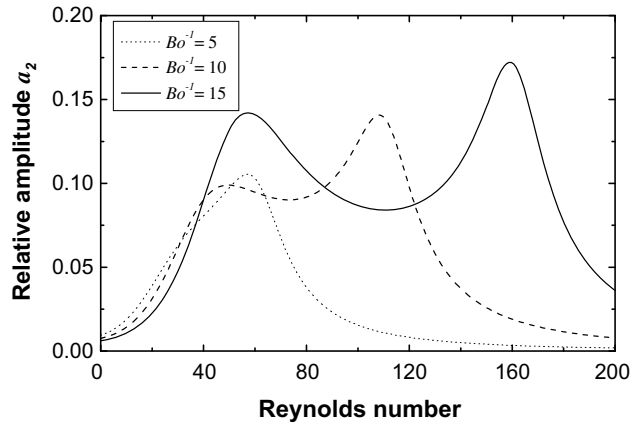

Fig. 10. Effect of the inverse Bond number on the relative free-surface amplitude. The other parameter values are: $\alpha = 13°$, $\delta = 0.3$, $\xi = 0.1$.

The solution at third order in the dimensionless wall amplitude yields a correction of the fundamental mode, obtained at first order, and a third harmonic of the bottom contour, as is apparent from (35). Fig. 11 shows the free-surface amplitude of the different contributions as a function of the Reynolds number. As in the case of the second-order solution, which yields the second harmonic, the solution for the third harmonic has additional peaks. The peak at highest Reynolds number is due to a resonance at

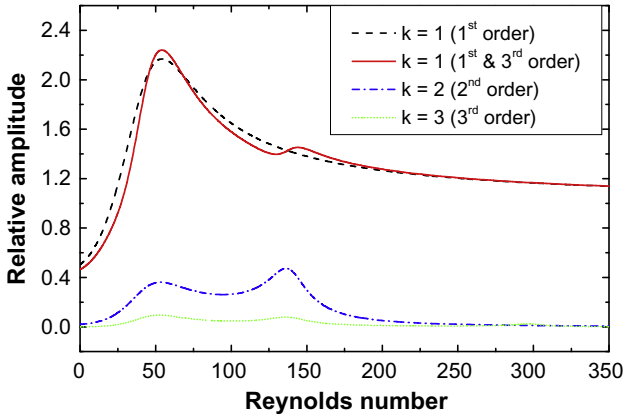

Fig. 11. Relative free-surface amplitude as a function of the Reynolds number. The other parameter values are: $\alpha = 13°$, $Bo^{-1} = 12.75$, $\delta = 0.3$, $\xi = 0.3$.

$$Re_3 = \frac{5}{2}(\cot\alpha + 9Bo^{-1}), \tag{48}$$

i.e. a resonance with capillary-gravity waves of a third of the wavelength of the bottom contour.

Peaks at lower Reynolds number are due to the coupling to the first and to the second-order solution and thus take place close to Reynolds numbers where these ones have local maxima. The contribution of the third-order solution to the fundamental wave number has only two maxima. This is apparently due to the fact that the resonance coincides with that of the first-order solution, i.e. it is at $Re_1 = 5/2(\cot\alpha + Bo^{-1})$. Thus it overlaps with the strong coupling to the first and second-order solutions. The second peak for the fundamental wave number is due to the coupling to the second-order solution.

4.4. Bistability

The analysis shows that the third-order solution in the dimensionless wall amplitude yields a correction to the fundamental wave-number result at first order. To see whether our reduced system still allows for bistable resonance we solved (24) numerically. Together with periodic boundary conditions, (24) is a third-order boundary-value problem which we solved using a finite-difference algorithm. As shown in Fig. 12, Eq. (24) shows indeed bistable resonance. Next we derive a generic nonlinear equation to study the main qualitative features of the bistability. The idea is to extend

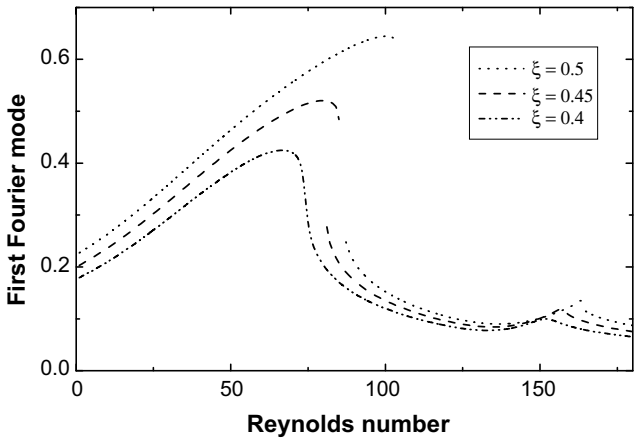

Fig. 12. First Fourier mode of the film thickness as a function of the Reynolds number for $\xi = 0.4, 0.45, 0.5$. The other parameters are: $Bo^{-1} = 5.7$, $\alpha = 15°$, $\delta = 0.3$.

the linear equation (26) with higher-order nonlinearities which have been skipped in the perturbation expansion. Therefore, we expand the film thickness into $F = 1 + \xi f_1$, where f_1 is written as a Fourier series $f_1 = c_1 \cos X + s_1 \sin X$ and consider only the fundamental wave number. Disregarding all higher harmonics results in

$$0 = (\delta \cot\alpha f_{1X} - \delta Bo^{-1} f_{1XXX})(1 + 3\xi^2 f_1^2) - \frac{2}{5} f_{1X} \delta Re - f_1(3 + \xi^2 f_1^2) - (1 + 3\xi^2 f_1^2)(\delta Bo^{-1} + \delta \cot\alpha) \sin X. \quad (49)$$

This is the nonlinear extension of the first-order equation for linear resonance (26). Three nonlinear terms arise: The first one is the hydrostatic and capillary-pressure term, the second one comes from the forcing due to the bottom undulation, and the third one takes into account higher-order corrections of the inhomogeneities. Parameter studies did not show any qualitative effect of the last two nonlinearities on the bistability. Here, we focus on the generic equation and thus we may neglect them in the following, arriving finally at

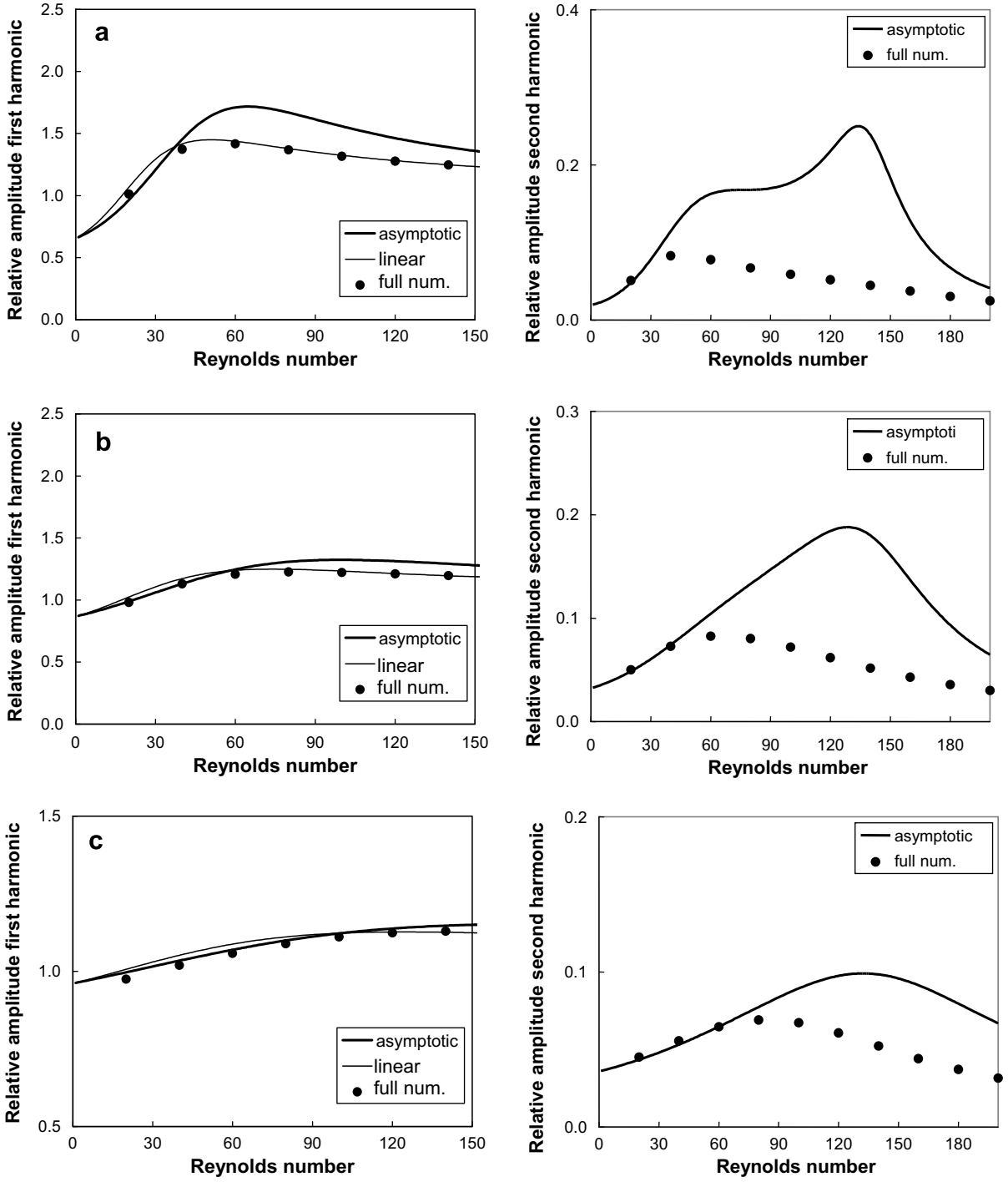

Fig. 13. Relative amplitude of the first and second harmonic for film-thickness $\delta = 0.2$ (a), 0.1 (b) and 0.05 (c) for fixed bottom geometry $2\pi a/\lambda = 0.05$. The other parameter values are: $\alpha = 13°$, $Bo^{-1} = 12.75$.

$$0 = (\delta\cot\alpha f_{1X} - \delta Bo^{-1} f_{1XXX})(1 + 3\xi^2 f_1^2) - \frac{2}{5} f_{1X}\delta Re - 3f_1 - (\delta Bo^{-1} + \delta\cot\alpha)\sin X. \quad (50)$$

Note that the hydrostatic and capillary pressure term has nonlinear contributions while the counteracting inertia term remains linear. This equation shows bistable resonance.

Although (50) is not an oscillator equation, it has the same type of solution as the driven nonlinear Duffing oscillator (Jordan and Smith, 1987), defined by $x_{tt} + 2\beta x_t + \omega^2 x + \varepsilon\omega^2 x^3 = f\cos\varpi t$, where β, f, ω, and ϖ are the damping constant, amplitude of the driving force, angular frequency of the oscillator and angular driving frequency, respectively. With the ansatz $x = A\cos(\varpi t - \Phi)$, the frequency response equation reads:

$$\left(A(\omega^2 - \varpi^2) + \varepsilon\frac{3}{4}\omega^2 A^3\right)^2 + (2\beta\varpi A)^2 = f^2, \quad (51)$$

for the amplitude and

$$\tan\Phi = 2\beta\varpi \Big/ \left(\omega^2 - \varpi^2 + \varepsilon\frac{3}{4}\omega^2 A^2\right), \quad (52)$$

for the phase lag. With the ansatz $f_1 = a_1\cos(X - \Delta\varphi_1)$, the solution of (50) takes the same form as (51) and (52) identifying

$$\omega^2 = \frac{1}{2}\delta\cot\alpha + \frac{1}{2}\delta Bo^{-1}, \quad \varpi^2 = \frac{1}{5}\delta Re, \quad 2\beta\varpi = \frac{3}{2}. \quad (53)$$

If the nonlinearity is present, the solution of (50) corresponds to that of a driven Duffing oscillator once substituting

$$\varepsilon = \xi^2. \quad (54)$$

5. Discussion and conclusions

We have studied nonlinear resonance in viscous gravity-driven films flowing over undulated substrates, numerically and analytically. The numerics have documented that, with increasing dimensionless wall amplitude, higher harmonics are generated on the free surface and then the resonance becomes bistable.

The asymptotic analysis has provided a qualitative understanding of these phenomena. In particular, it has revealed that higher harmonics are generated by the nonlinear coupling of the wall with lower-order harmonics of the free surface. The asymptotic analysis has also accounted for bistable resonance in flows over steep bottom undulations. The solution of a minimum model retaining the essential nonlinearities responsible for bistabilty is similar to that of the Duffing oscillator.

To investigate systematically the range of validity of the asymptotics, we compare the analytical results with numerics of the full field equations and the linear theory in Wierschem et al. (2008) for various values of dimensionless film thickness. The results are shown in Fig. 13, and refer to $\alpha = 13°$, $Bo^{-1} = 12.75$. It has to be noted that we exceeded the validity domain for the linear prediction of Wierschem et al. (2008) and the present asymptotics in Fig. 13(b) and (c). Although $\xi = O(1)$, we obtain satisfactory qualitative agreement with the numerical results. We observe that the asymptotic prediction of the first harmonic is acceptable even for the thicker film $\delta = 0.2$, and improves uniformly with decreasing δ. On the contrary, the prediction of the second harmonic is quantitatively correct only in a range of low Reynolds numbers, whose width increases with decreasing δ. The deviation at high Re is significant and in particular overestimates the second-order resonance.

The discrepancy at second order is again explained by considering that the actual film thickness for the second harmonic is twice the nominal, and, consequently, the actual inverse Bond number for the second-order resonance is four times the nominal. We conclude that asymptotic analysis reveals correctly the dominant nonlinear mechanisms and provides quantitatively satisfactory first-order estimates for thin films. However, its accuracy deteriorates fast at higher harmonics.

Acknowledgements

We acknowledge the comments and suggestions made by the anonymous referees.

Appendix A. Third-order solution

The inhomogeneities at third order in ξ (Eq. (36)) are:

$$M_{31} = \frac{1}{6}\left(\left(-\frac{18}{5}M_2C_1 - \frac{9}{5}MS_1 - \frac{9}{5}NC_1 + \frac{9}{5}S_1^2C_1 + \frac{9}{5}C_1^3\right)\delta Re + 36M_2S_1 - \frac{45}{2}S_1C_1^2 - \frac{45}{2}S_1^3 - 18NS_1 + 18MC_1\right),$$

$$N_{31} = \frac{1}{6}\left(\left(\frac{18}{5}M_2S_1 - \frac{9}{5}NS_1 + \frac{9}{5}MC_1 - \frac{9}{5}S_1^3 - \frac{9}{5}C_1^2S_1\right)\delta Re - \frac{45}{2}C_1^3 - \frac{45}{2}S_1^2 + 18NC_1 + 36M_2C_1 + 18MS_1\right),$$

$$M_{33} = \frac{1}{6}\left(\left(\frac{27}{5}MS_1 - \frac{27}{5}NC_1 - \frac{27}{5}S_1^2C_1 + \frac{9}{5}C_1^3\right)\delta Re + \frac{15}{2}S_1^3 - \frac{45}{2}S_1C_1^2 + 18MC_1 + 18NS_1\right),$$

$$N_{33} = \frac{1}{6}\left(\left(\frac{27}{5}NS_1 + \frac{27}{5}MC_1 + \frac{9}{5}S_1^3 - \frac{27}{5}S_1C_1^2\right)\delta Re - \frac{15}{2}C_1^3 + \frac{45}{2}S_1^2C_1 + \frac{45}{2}S_1^2C_1 + 18NC_1 - 18MS_1\right).$$

References

Aksel, N., 2000. Influence of the capillarity on a creeping film flow down an inclined plane with an edge. Arch. Appl. Mech. 70, 81–90.

Alekseenko, S.V., Nakoryakov, V.Y., Pokusaev, B.G., 1985. Wave formation on a vertical falling liquid film. AIChE 31, 1446–1461.

Argyriadi, K., Vlachogiannis, M., Bontozoglou, V., 2006. Experimental study of inclined film flow along periodic corrugations: the effect of wall steepness. Phys. Fluids 18, 012102.

Blyth, M.G., Pozrikidis, C., 2006. Film flow down an inclined plane over a three-dimensional obstacle. Phys. Fluids 18, 052104.

Bontozoglou, V., 2000. Laminar film flow along a periodic wall. CMES 1, 133–142.

Bontozoglou, V., Papapolymerou, G., 1997. Laminar film flow down a wavy incline. Int. J. Multiphase Flow 23, 69–79.

Chang, H.-C., Demekhin, E.A., 2002. Complex Wave Dynamics on Thin Films. Elsevier, Amsterdam.

Davalos-Orozco, L.A., 2007. Nonlinear instability of a thin film flowing down a smoothly deformed surface. Phys. Fluids 19, 074103.

Davis, J.M., Troian, S.M., 2005. Generalized linear stability of noninertial coating flows over topographical features. Phys. Fluids 17, 072103.

Gaskell, P.H., Jimack, P.K., Sellier, M., Thompson, H.M., Wilson, M.C.T., 2004. Gravity-driven flow of continuous thin liquid films on nonporous substrates with topography. J. Fluid Mech. 509, 253–280.

Gaskell, P.H., Jimack, P.K., Sellier, M., Thompson, H.M., 2006. Flow of evaporating, gravity-driven thin liquid films over topography. Phys. Fluids 18, 013601.

Jordan, D.W., Smith, P., 1987. Nonlinear Ordinary Differential Equations, second ed. Oxford University Press, Oxford.

Kabova, Yu.O., Alexeev, A., Gambaryan-Roisman, T., Stephan, P., 2006. Marangoni-induced deformation and rupture of a liquid film on a heated micro-structured wall. Phys. Fluids 18, 012104.

Kalliadasis, S., Bielarz, C., Homsy, G.M., 2000. Steady free-surface thin film flows over topography. Phys. Fluids 12, 1889–1898.

Luo, H.X., Pozrikidis, C., 2006. Effect of inertia on film flow over oblique and three-dimensional corrugations. Phys. Fluids 14, 078107.

Luo, H.X., Pozrikidis, C., 2007. Gravity-driven film flow down an inclined wall with three-dimensional corrugations. Acta Mech. 188, 209–225.

Malamataris, N.A., Vlachogiannis, M., Bontozoglou, V., 2002. Solitary waves on inclined films: flow structure and binary interactions. Phys. Fluids 14, 1082–1094.

Matar, O.K., Craster, R.V., Kumar, S., 2007. Falling films on flexible inclines. Phys. Rev. E 76, 056301.

Mazouchi, A., Homsy, G.M., 2001. Free surface Stokes flow over topography. Phys. Fluids 13, 2751–2761.

Nguyen, L.T., Balakotaiah, V., 2000. Modeling and experimental studies of wave evolution on free-falling viscous films. Phys. Fluids 12, 2236–2256.

Oron, A., Heining, C., 2008. Weighted-residual integral boundary-layer model for the nonlinear dynamics of thin liquid films falling on an undulating vertical wall. Phys. Fluids 20, 082102.

Pohlhausen, K., 1921. Zur näherungsweisen Integration der Differentialgleichung der laminaren Reibungsschicht. ZAMM 1, 252–268.

Pozrikidis, C., 1988. The flow of a liquid film along a periodic wall. J. Fluid Mech. 188, 275–300.

Pozrikidis, C., 2003. Effect of surfactants on film flow down a periodic wall. J. Fluid Mech. 496, 105–127.

Prokopiou, T., Cheng, M., Chang, H.-C., 1991. Long waves on inclined films at high Reynolds number. J. Fluid Mech. 222, 665–691.

Roberts, A.J., Li, Z., 2006. An accurate and comprehensive model of thin fluid flows with inertia on curved substrates. J. Fluid Mech. 553, 33–73.

Ruyer-Quil, C., Manneville, P., 2002. Further accuracy and convergence results on the modeling of flows down inclined planes by weighted-residual approximations. Phys. Fluids 14, 170–183.

Salamon, T.R., Armstrong, R.C., Brown, R.A., 1994. Traveling waves on vertical films: numerical analysis using the finite-element method. Phys. Fluids 6, 2202–2220.

Shkadov, W.Y., 1967. Wave conditions in the flow of a thin layer of a viscous liquid under the action of gravity. Izv. Akad. Nauk. SSSR, Mekh. Zhidk. Gaza 1, 43–50.

Spurk, J.H., Aksel, N., 2007. Fluid Mechanics, second ed. Springer, Berlin.

Trifonov, Y.Y., 1998. Viscous liquid film flows over a periodic surface. Int. J. Multiphase Flow 24, 1139–1161.

Trifonov, Y.Y., 2007. Stability of a viscous liquid film flowing down a periodic surface. Int. J. Multiphase Flow 33, 1186–1204.

Tseluiko, D., Blyth, M.G., Papageorgiou, D.T., Vanden-Broeck, J.M., 2008a. Electrified viscous thin film flow over topography. J. Fluid Mech. 597, 449–475.

Tseluiko, D., Blyth, M.G., Papageorgiou, D.T., Vanden-Broeck, J.M., 2008b. Effect of an electric field on film flow down a corrugated wall at zero Reynolds number. Phys. Fluids 20, 042103.

Uecker, H., 2004. Self-similar decay of spatially localized perturbations in the integral boundary layer equation. J. Diff. Eq. 207, 407–422.

Valluri, P., Matar, O.K., Hewitt, G.F., Mendes, M.A., 2005. Thin film flow over structured packings at moderate Reynolds numbers. Chem. Eng. Sci. 60, 1965–1975.

Vlachogiannis, M., Bontozoglou, V., 2002. Experiments on laminar film flow along a periodic wall. J. Fluid Mech. 457, 133–156.

von Kármán, Th., 1921. Über laminare und turbulente Reibung. ZAMM 1, 233–252.

Wierschem, A., Aksel, N., 2003. Instability of a liquid film flowing down an inclined wavy plane. Physica D 186, 221–237.

Wierschem, A., Aksel, N., 2004a. Hydraulic jumps and standing waves in gravity-driven flows of viscous liquids in wavy open channels. Phys. Fluids 16, 3868–3877.

Wierschem, A., Aksel, N., 2004b. Influence of inertia on eddies created in films creeping over strongly undulated substrates. Phys. Fluids 16, 4566–4574.

Wierschem, A., Scholle, M., Aksel, N., 2002. Comparison of different theoretical approaches to experiments on film flow down an inclined wavy channel. Exp. Fluids 33, 429–442.

Wierschem, A., Scholle, M., Aksel, N., 2003. Vortices in film flow over strongly undulated bottom profiles at low Reynolds numbers. Phys. Fluids 15, 426–435.

Wierschem, A., Lepski, C., Aksel, N., 2005. Effect of long undulated bottoms on thin gravity-driven films. Acta Mech. 179, 41–66.

Wierschem, A., Bontozoglou, V., Heining, C., Uecker, H., Aksel, N., 2008. Linear resonance in viscous films on inclined wavy planes. Int. J. Multiphase Flow 34, 580–590.

Zhao, L., Cerro, R.I., 1992. Experimental characterization of viscous film flows over complex surfaces. Int. J. Multiphase Flow 18, 495–516.